Osmotic actuation modelling for innovative biorobotic solutions inspired by the plant kingdom

2013 Bioinspir. Biomim. 8 025002

(http://iopscience.iop.org/1748-3190/8/2/025002)

Bioinspir. Biomim. **8** (2013) 025002 (12pp) doi:10.1088/1748-3182/8/2/025002

Osmotic actuation modelling for innovative biorobotic solutions inspired by the plant kingdom

E Sinibaldi[1], G L Puleo[1], F Mattioli[1,2], V Mattoli[1], F Di Michele[1], L Beccai[1], F Tramacere[1,2], S Mancuso[3] and B Mazzolai[1]

[1] Center for Micro-BioRobotics@SSSA, Istituto Italiano di Tecnologia, Viale Rinaldo Piaggio 34, I-56025 Pontedera, Italy

[2] The BioRobotics Institute, Scuola Superiore Sant'Anna, Viale Rinaldo Piaggio 34, I-56025 Pontedera, Italy

[3] Department of Plant, Soil and Environment, University of Florence, Viale delle Idee 30, I-50019 Sesto F.no, Florence, Italy

E-mail: barbara.mazzolai@iit.it

Received 27 August 2012
Accepted for publication 27 March 2013
Published 7 May 2013
Online at stacks.iop.org/BB/8/025002

Abstract

Osmotic-driven plant movements are widely recognized as impressive examples of energy efficiency and low power consumption. These aspects motivate the interest in developing an original biomimetic concept of new actuators based on the osmotic principle exploited by plants. This study takes a preliminary step in this direction, by modelling the dynamic behaviour of two exemplificative yet relevant implementations of an osmotic actuator concept. In more detail, the considered implementations differ from each other in the way actuation energy storage is achieved (through a piston displacement in the former case, through membrane bulging in the latter). The dynamic problem is analytically solved for both cases; scaling laws for the actuation figures of merit (namely characteristic time, maximum force, maximum power, power density, cumulated work and energy density) as a function of model parameters are obtained for the bulging implementation. Starting from such performance indicators, a preliminary dimensioning of the envisaged osmotic actuator is exemplified, based on design targets/constraints (such as characteristic time and/or maximum force). Moreover, model assumptions and limitations are discussed towards effective prototypical development and experimental testing. Nonetheless, this study takes the first step towards the design of new actuators based on the natural osmotic principle, which holds potential for disruptive innovation in many fields, including biorobotics and ICT solutions.

(Some figures may appear in colour only in the online journal)

1. Introduction

Most plants appear to lack the contractile proteins used in the energy demanding processes for movement found in animals (Dumais and Forterre 2012). Although plants lack muscles and are typically considered stationary, they generate a diversity of non-muscular movements that allow them, for example, to efficiently explore the environment, looking for nutrients and avoiding possible dangers, or to spread around their genetic material, ensuring species continuity and diversification. These kinds of movements present many appealing characteristics: remarkable energy efficiency (gained during the evolution process over almost half a billion of years), high actuation force and a rich motion repertoire (a successful strategy supporting survival in different and challenging conditions). Driven by these considerations, since the pioneering work of the Darwins (Darwin 1875, Darwin and Darwin 1880), the question of how plants move in the absence of muscles has attracted the interest of many scientists (Jost and Gibson 1907, Ruhland 1959, Hart 1990). From a biological perspective, the physiology of plant movements is central to the understanding of plant development and plant responses to environmental stimuli such as light and gravity (Gilroy and Masson 2008, Moulia and Fournier 2009). Moreover, suitable comprehension of these non-muscular movements holds potential for developments in applied sciences and engineering as well, in particular, in view of the creation of novel biomimetic actuation strategies, characterized by high energy efficiency and low power consumption (Taya 2003, Burgert and Fratzl 2009, Martone *et al* 2010).

Plant movements can be mainly classified into two main categories, namely active and passive movements, depending on the associated generation mechanisms (Hill and Findlay 1981). In particular, active systems are based on living cells that activate and control the response by moving ions and changing the permeability of membranes on the base of action potentials (Simons 1981, Sibaoka 1991, Fromm and Lautner 2007, Moran 2007, Uehlein and Kaldenhoff 2008). Conversely, passive systems are mostly based on dead tissues that are suitably structured to undergo predetermined modifications upon changes under environmental conditions (Fahn and Werker 1972, Burgert and Fratzl 2009).

Within the active movements category, nastic movements, defined as non-directional responses to stimuli, offer surprising performances in terms of both speed and active pressure. A few illuminating examples include the rapid (∼50 ms) closure of *Dionaea muscipula* (Venus flytrap), partly actuated by an abrupt decrease of internal tissue pressure (Forterre *et al* 2005, Burgert and Fratzl 2009); the leaf closure by touch stimuli in *Mimosa pudica*, that occurs within 20 ms from when they are touched (Oda and Abe 1972); the *Stylidium* impressive pollination mechanism, where Gynostaemium flips rapidly (∼25 ms) to hit and pollinate insects (Hill and Findlay 1981); and the remarkable 4.5 MPa actuation pressure exhibited by stomatal guard cells during the closing phase, aimed at containing water loss (Hill and Findlay 1981, Roelfsema and Hedrich 2002).

While predation, self-defence, reproduction and water retention can justify the use of the aforementioned motion strategies, the efficient exploration of the environment and the search for nutrients are fundamental for plant survival. Indeed, soil penetration represents an outstanding adaptive reply to the quest for resources: plant roots are able to autonomously and efficiently move, surrounded by the soil, and to modify their behaviour based on the environment characteristics. In particular, roots are able to also penetrate strong mechanical impedance media, by continuously exerting a pressure on the order of 1 MPa, while elongating over lengths up to 10 m (Popova *et al* 2012, Green *et al* 1971, Zhu and Boyer 1992). Such a penetration task is energy demanding, yet it can be accomplished by plant roots more efficiently than by muscle-driven drilling systems, by virtue of their turgor-based actuation strategy.

Turgor pressure (P) can be regarded as a sort of 'natural hardness' generated by the water flux into the roots' cells along the water potential gradient sustained by the osmotic pressure difference. Quantitatively speaking, turgor pressure can be described by the relation $P = \pi_o - \pi_i$, where π_i is the osmotic potential inside the cell and π_o represents the osmotic potential outside the cell (Bengough *et al* 1997). This equation assumes that water influx into the cell is not upper-bounded, there is no transpiration tension and solutes have a reflection coefficient near unity (Pritchard 1994).

From a functional viewpoint, natural osmotic systems rely on four main elements: an osmotic membrane, a rigid structure, a compliant transducer and a suitable osmotic power reservoir. The stiff plant cell, made of highly organized cellulose microfibrils embedded in a pectin matrix bears the main responsibility for osmotic pressure formation in plant roots (Preston 1974, Taiz and Zeiger 2002, Baskin 2005). From a biomechanical viewpoint, this complex polymeric system, without considering any active transport and gate proteins, plays a twofold function

- it constitutes the most part of the natural osmotic membrane (exhibiting good solute rejection properties and good water permeability); and
- it acts as a first level transducer for actuation power through its pressure-driven deformation (Dumais and Forterre 2012).

Furthermore, cell deformation under osmotic potential is mainly isotropic; nonetheless, directional actuation can be obtained through the mediation of additional stiff elements (e.g. lignin rich structure, dead tissue), of metastable structures or by means of specific biochemical mechanisms (e.g. auxin mechanism, special osmotic metabolism, osmotic agent active transport) (Dumais and Forterre 2012). Clearly, in such a framework, an osmotic power reservoir is successfully provided by soil presence and cell proximity (Steudle and Peterson 1998).

As anticipated above, plant roots greatly exploit passive osmosis, in which osmotic pressure is generated by solvent flux across a semi-permeable membrane (i.e. cell wall), from a region of higher solvent chemical potential (i.e. lower solute concentration) to a region of lower solvent chemical potential (i.e. higher solute concentration). The basic principles of the osmotic process are known from fundamental physics. In particular, solvent transport across the membrane is inhibited by applying a pressure directly opposing the osmotic one to the volume of the most concentrated solution. Moreover, classic thermodynamics describes the osmotic pressure difference Π for a completely dissociated electrolyte in solution at equilibrium as $\Pi = iRT \log{(1-x)}/V_m$, where i is the number of ions for formula unit, R is the universal gas constant ($R = 8.314$ J K^{-1} mol^{-1}), T denotes absolute temperature, x is the solute molar fraction difference between the chamber solutions and V_m represents the solvent molar volume. For ideal solutions, the aforementioned relation simplifies to (Atkins 1994)

$$\Pi = iRTM, \tag{1}$$

also known as the van't Hoff formula, where M denotes the molarity concentration difference between the chamber solutions.

A number of technological approaches has been proposed in order to control the osmotic process by means of additional physical mechanisms, such as, for instance, those related to water desalination (Cath *et al* 2006) and power generation (Skilhagen *et al* 2008) or in electro-osmotic applications (Andersson and van den Berg 2003, Piyasena *et al* 2009). Among them, relevant studies also addressed actuation (Wang *et al* 2012), and the development of mechatronic systems based on such an actuation (Mazzolai *et al* 2011). However, technical complexity usually related to the implementation of effective actuation systems motivates the development of actuation strategies that only rely on the osmotic process *per se*. As regards to our knowledge, only a few relevant background references can be found in the literature. One work dates back to the early 1970s and it is now recognized as the basic principle of macroscale osmotic pumps for drug delivery (Theeuewes and Yum 1976); it mainly addressed the transduction of osmotic pressure potential into squeezing movements. Another example was recently proposed (Su *et al* 2002), and concerns an osmotic actuator for osteogenesis controlled distraction and drug release (Li and Su 2010). Both the aforementioned systems are mainly passively controlled, based on the main characteristics of their working environment, and this aspect poses some limitations on the achievable actuation performance. Nevertheless, despite the complexity related to its development, an osmosis-based actuation system could outperform traditional solutions, being characterized by low power consumption, high actuation force and architectural features suitable to exploit favourable scale effects, similar to phenomena observed in Nature.

In this work, we get inspiration from plants and we investigate the osmotic principle with the aim of bringing new insights for innovative, energy efficient and low power actuation solutions. With such an objective in mind, in section 2 we introduce an osmotic actuator concept, together with a simple model able to describe its dynamics. In more detail, we consider two exemplificative yet relevant implementations, which only differ from each other in the way actuation energy storage is achieved. We analytically solve the dynamic problem for both cases, yet we only elaborate on the latter one (involving membrane bulging), by virtue of its potential for effective prototypical development and experimental testing. Relevant derivations for such a model are reported in the appendix, for ease of readability, together with the expression of the main actuation performance indicators. Then, in section 3, we use the model in order to outline some basic design considerations. In particular, a preliminary dimensioning of the envisaged osmotic actuator is exemplified, based on design targets/constraints (such as characteristic time and/or maximum force). Main take home messages are also highlighted. Finally, concluding remarks are reported in section 4.

2. Materials and methods

A basic model is introduced in the present section, aimed at analysing the relevant features of the envisaged osmotic actuation concept, in view of specific design configurations to be studied after such a conceptual, icebreaking phase.

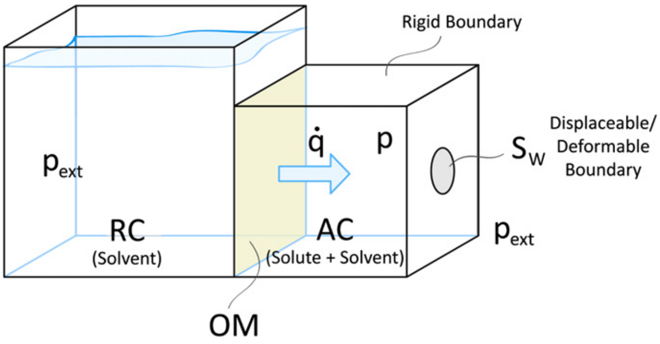

Figure 1. Schematic of the osmotic actuator concept showing the reservoir chamber (RC), the actuation chamber (AC) and the osmotic membrane (OM). The displaceable portion of the AC boundary is introduced for storing/gathering the energy associated with the osmotic process. Solvent flux $\dot{q}$ is also sketched.

At this stage we represent the actuator as the two-chamber system shown in figure 1: the solvent contained within the reservoir chamber (RC) can flow towards the actuation chamber (AC), also containing solute, through the osmotic membrane (OM). The AC represents the main working domain in the present model: we assume that, at the initial time $t_0 = 0$, its volume V_0 contains a number n of solute moles so that a corresponding molar concentration $M_0 = n/V_0$ contributes as an osmotic flux driver at t_0. Moreover, some degree of approximation is introduced for ease of presentation, namely:

- (h0) solvent flux occurs through the whole OM surface during the considered observation time;
- (h1) the OM perfectly allows for solvent transport while being impermeable to solute flux;
- (h2) the OM characteristics do not change over the considered observation time;
- (h3) surface effects close to the OM play a minor role so that bulk solute concentration mainly contributes as osmotic flux driver;
- (h4) OM deformation during the observation time is negligible;
- (h5) solvent compressibility can be neglected.

Clearly, assumption (h0) does not weaken model generality (RC being conceived as a reservoir). Furthermore, (h5) is readily motivated by the fact that—for practical implementations—the energy associated with the osmotic actuation process is mainly stored/gathered through the displacement/deformation of a portion S_w of the AC boundary (see figure 1 and subsections below), whose compliance can be assumed much greater than that of the working solvent (water could be assumed in this regard to fix ideas). The remaining simplifying assumptions are discussed in section 3.

Under the above assumptions, solvent flux $\dot{q}$ across the OM is simply given by (Cath *et al* 2006)

$$\dot{q} = S_{\mathrm{OM}}\alpha_{\mathrm{OM}}(\Pi + p_{\mathrm{RC}} - p), \tag{2}$$

where S_{OM} and α_{OM} respectively denote the surface area and the permeability of the OM; p_{RC} and p denote pressure within

RC and AC, respectively; and Π indicates the osmotic pressure difference between AC and RC.

Without major losses of generality, we can assume $p_{\mathrm{RC}} \cong p_{\mathrm{ext}}$, where p_{ext} denotes the external environment pressure. Moreover, once the volume $V = V(t)$ of the AC at time t is introduced (explicit dependence on t is hereafter dropped, for ease of conciseness), it is straightforward to describe its time variation as $\mathrm{d}V/\mathrm{d}t = \dot{q}$, and to update the AC molar concentration as $M = n/V = M_0V_0/V$. Hence, by recalling equation (1), the osmotic pressure difference is given by $\Pi = \Pi_0 V_0/V$ (the van't Hoff approximation surely fits the present modelling framework). Moreover, equation (2) straightforwardly leads to the following ordinary differential equation:

$$\frac{\mathrm{d}V}{\mathrm{d}t} = S_{\mathrm{OM}}\alpha_{\mathrm{OM}}\left[\Pi_0\frac{V_0}{V} + p_{\mathrm{ext}} - p\right], \tag{3}$$

which describes the AC volume variation starting from $V(0) = V_0$.

An additional relation linking pressure p to volume V is needed in order to determine the actuation dynamics. Such a relation clearly depends on the specific mechanism introduced within the AC for storing/transferring the osmotic actuation work through the displacement/deformation of S_w. In a practical implementation, such an element must be able to transfer (at least part of) the work produced by the osmotic process to a movable structure, which is in turn capable of performing actuation on the environment. However, in this study it is suitable to consider a displacement/deformation of S_w leading to a non-dissipative energy storage mechanism. Indeed, besides allowing for some degree of generality (through the independence from specific load conditions), such a position also permits us to easily exploit the displacement/deformation of S_w for measuring some performance metrics, as discussed below. In particular, two relevant, though exemplificative, implementations of the osmotic actuator concept are respectively discussed in sections 2.1 and 2.2, which are characterized by two different ways of achieving storage of the osmotic actuation work. We present analytical solutions for both implementations, yet we only elaborate on the latter, in the light of its potential for effective prototypical development and experimental testing.

Before focusing on model development, it is worth remarking that the key elements defining the envisaged osmotic actuation concept are four: the OM, the rigid structure of the AC, the deformable part of the AC (here presented as an energy storage element, yet to be also considered as a force transducer) and the osmotic potential reservoir (granted by the presence of the RC in combination with the initial osmotic pressure difference). It should be noted that these very elements also come into play when considering osmotic actuation in plant roots (see section 1), by allowing for some modifications (e.g. root cell wall simultaneously acts as the OM and force transducer).

2.1. Osmotic actuator dynamic model I (energy storage through an external elastic load)

In the first exemplificative implementation of the considered osmotic actuator concept, the actuation work is stored through

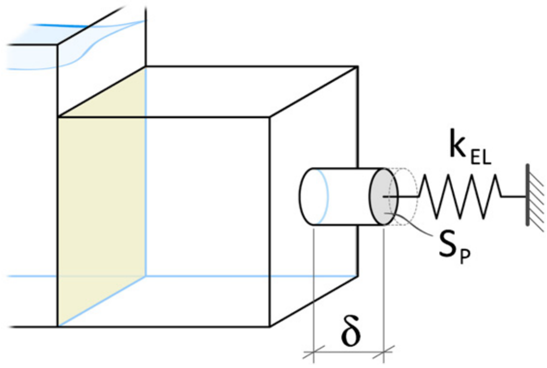

Figure 2. Exemplificative implementation of the osmotic actuator concept: actuation work is stored through the elastic deformation of an external load.

the elastic deformation of an external load. In particular, a piston is introduced, running along a straight cylindrical guide with a cross-section area S_p as in figure 2 (clearly, the AC displaceable boundary S_w is here represented by the sliding base surface of the piston).

The piston displacement δ is governed by solvent flux and it is trivially provided by the mass conservation law, namely $\delta = (V - V_0)/S_p$. Moreover, by assuming that inertial and friction effects associated with piston motion are negligible (as for quasi-static piston displacement), momentum balance for the piston provides the relation $(p - p_{\mathrm{ext}})\, S_p = k_{\mathrm{EL}}\delta$, where k_{EL} denotes the external load stiffness. The above relations permit us to recast equation (3) as follows:

$$\frac{\mathrm{d}V}{\mathrm{d}t} = S_{\mathrm{OM}}\alpha_{\mathrm{OM}}\left[\Pi_0\frac{V_0}{V} - \frac{k_{\mathrm{EL}}}{S_{\mathrm{p}}^2}(V - V_0)\right]. \tag{4}$$

Equation (4) can thus be integrated, starting from the initial condition $V(0) = V_0$.

To this purpose, once the reference time $\bar{t} := S_p^2/(k_{\mathrm{EL}}S_{\mathrm{OM}}\alpha_{\mathrm{OM}})$ and the non-dimensional coefficient $C := \Pi_0 S_p^2/(V_0 k_{\mathrm{EL}})$ are introduced, it is possible to rewrite equation (4) and its initial condition so as to describe the evolution of the non-dimensional volume $v := V/V_0$ against non-dimensional time $\tau := t/\bar{t}$, namely

$$\frac{\mathrm{d}v}{\mathrm{d}\tau} = C\frac{1}{v} - (v-1), \quad v(0) = 1. \tag{5}$$

Classical arguments (see e.g. Ince 1956) show that the solution of problem (5) monotonically increases from the initial value up to a regime value v_∞. More precisely, once $\omega = \omega(C) := \sqrt{1+4C}$, $v_1^* = v_1^*(C) := (1+\omega)/2$ and $v_2^* = v_2^*(C) := (1-\omega)/2$ are defined, it can be seen that $v_\infty = v_1^*$ (indeed, v_1^* and v_2^* are the roots of the steady-state equation $v^{*2} - v^* - C = 0$, yet only v_1^* is positive and therefore physically admissible). Moreover, problem (5) can be integrated by the separation of variables (see the appendix for more details on this technique), thus obtaining the following non-dimensional solution:

$$2\tau = \log_{\mathrm{e}}\left[\frac{\Psi(1;C)}{\Psi(v;C)}\right] \tag{6a}$$

where

$$\Psi(\xi;C) := \left(v_1^* - \xi\right)^{1+1/\omega}\left(\xi - v_2^*\right)^{1-1/\omega}. \tag{6b}$$

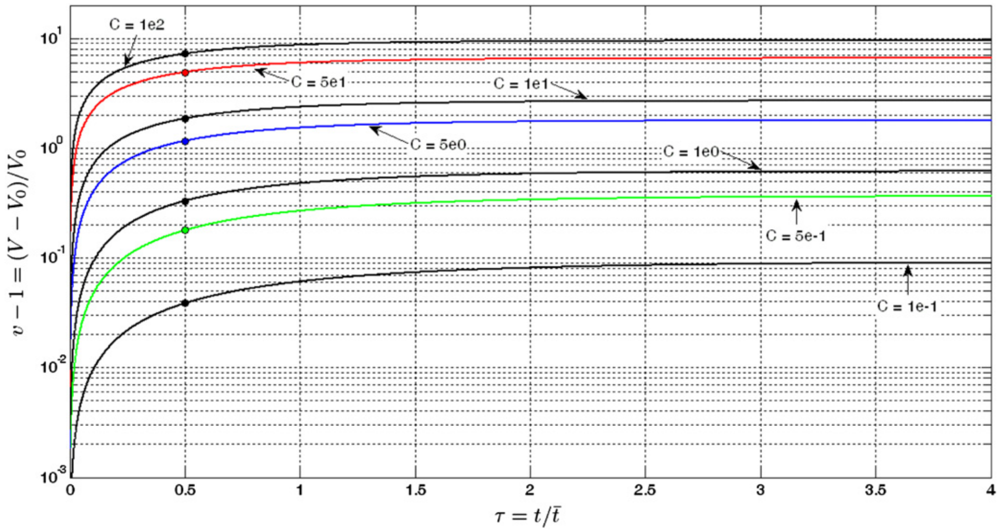

Figure 3. Exemplificative trends of the AC volume increment versus time (non-dimensional quantities), as obtained from the solution (6).

It should be noted that, for the considered implementation, the regime value v_∞ only depends on C, namely $v_\infty = \left(1+\sqrt{1+4C}\right)/2$. Moreover, a characteristic time $t_{c,p}$ associated with the considered 'damped' dynamics can be derived from the left-hand-side term of equation (6*a*) by imposing $2\tau = t/t_{c,p}$, thus obtaining $t_{c,p} = \bar{t}/2$ (it only depends on $\bar{t}$ for the present case). Exemplificative trends for the obtained solution are shown in figure 3, for some values of the parameter C. For each curve, the filled circle is associated with the characteristic non-dimensional time $t_{c,p}/\bar{t}$.

Despite its simplicity, the considered model permits us to directly link, e.g., characteristic actuation time and AC volume increase at regime to the free parameters $\bar{t}$ and C. Additional figures of merit, such as maximum actuation force, power density and energy density, can be derived from the obtained solution. However, such a derivation is not carried out here, for ease of presentation (conversely, it is introduced for the implementation discussed in section 2.2).

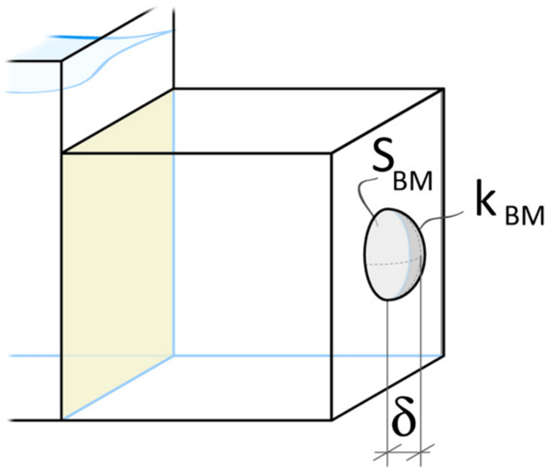

Figure 4. Exemplificative implementation of the osmotic actuator concept: actuation work is stored through the elastic deformation of a bulging membrane (also preventing solvent leakages).

2.2. Osmotic actuator dynamic model II (energy storage through elastic membrane bulging)

A further exemplificative implementation of the considered osmotic actuator concept is based on a deformable membrane, covering in particular the deformable boundary portion S_w shown in figure 2. The considered membrane bulges due to solvent flux, and a regime configuration can be reached provided that internal membrane tension can bear the pressure difference $p - p_{\text{ext}}$ locally acting on the membrane surface, as sketched in figure 4. Hence, as long as membrane deformation remains within the elastic domain, work associated with the osmotic actuation mechanism is stored as elastic energy in the membrane structure. Before tackling model derivations, it is worth remarking that the implementation at hand holds potential for effective prototypical development and experimental testing. Indeed, besides acting as an energy storage (and possibly force transduction) element, the bulging membrane might also lead to a favourable implementation by preventing solvent leakages from the AC in a rather simple way.

Let us assume that the displaceable boundary S_w shown in figure 2 is a circle with radius r, so that the footprint area of the bulging membrane is $S_{\text{BM}} = \pi r^2$. Moreover, let the bulge geometry be classically approximated through a spherical shape, in order to obtain simple expressions for bulge height δ and for the corresponding membrane tension (Small and Nix 1992). In more detail, provided that $\delta/r \ll 1$, bulge volume V_{BM} (governed by solvent flux) can be approximated as $V_{\text{BM}} \cong S_{\text{BM}}\delta/2$. Moreover, linear elastic theory provides the following relation from the membrane momentum balance (Timoshenko 1964) (by assuming a uniform, biaxial tensional state): $p - p_{\text{ext}} \cong (8Y_{\text{BM}}t_{\text{BM}}\delta^3)/(3r^4) = (8\pi^2 Y_{\text{BM}}t_{\text{BM}}\delta^3)/(3S_{\text{BM}}^2)$, where Y_{BM} and t_{BM} respectively denote membrane biaxial modulus and thickness. The former parameter, in particular, can be defined from the Young modulus E and the Poisson coefficient ν as follows: $Y := E/(1-\nu)$. By combining the above expressions, we obtain $p - p_{\text{ext}} \cong \left(64\pi^2 Y_{\text{BM}}t_{\text{BM}}V_{\text{BM}}^3\right)/\left(3S_{\text{BM}}^5\right)$

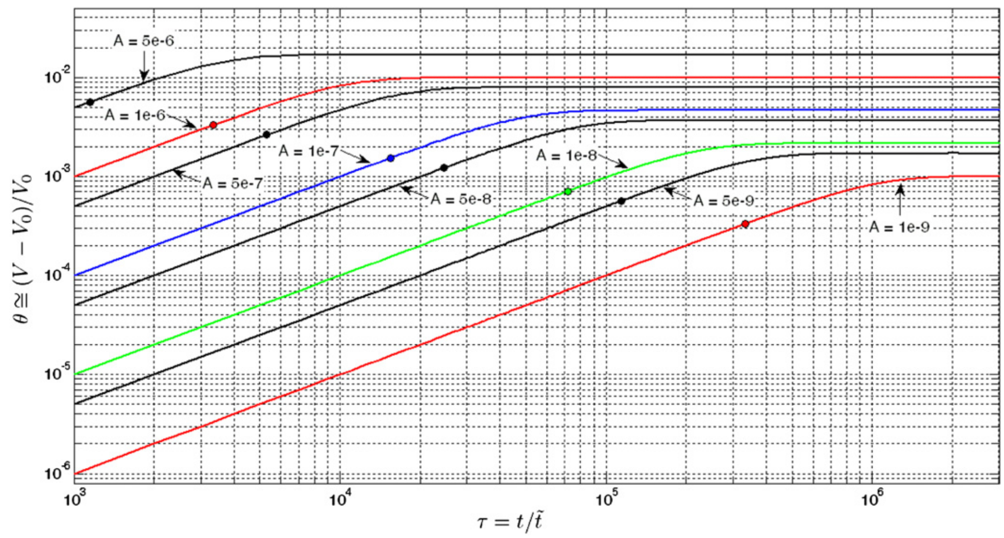

Figure 5. Exemplificative trends of the bulge volume versus time (non-dimensional quantities), as obtained from the solution (9).

and, by observing that $V_{\mathrm{BM}} = V - V_0$, it is straightforward to rewrite equation (3) as follows:

$$\frac{\mathrm{d}V}{\mathrm{d}t} = S_{\mathrm{OM}}\alpha_{\mathrm{OM}}\left[\Pi_0\frac{V_0}{V} - \frac{k_{\mathrm{BM}}}{S_{\mathrm{BM}}^5}(V - V_0)^3\right], \qquad (7)$$

where $k_{\mathrm{BM}} := 64\pi^2 Y_{\mathrm{BM}} t_{\mathrm{BM}}/3$ represents a membrane stiffness coefficient. Equation (7) can then be integrated, starting from the initial condition $V(0) = V_0$. Moreover, physical representativeness of the corresponding solution must be systematically checked with respect to the working hypothesis of small bulging deformations ($\delta/r \ll 1$) originally exploited in order to formulate the proposed model.

In more detail, once both the reference time $\tilde{t} := S_{\mathrm{BM}}^5/\left(k_{\mathrm{BM}}S_{\mathrm{OM}}\alpha_{\mathrm{OM}}V_0^2\right)$ and the non-dimensional coefficient $A := \Pi_0 S_{\mathrm{BM}}^5/\left(V_0^3 k_{\mathrm{BM}}\right)$ are introduced, it is possible to recast equation (7) and its initial condition so as to describe the evolution of the non-dimensional bulge volume $\epsilon := V_{\mathrm{BM}}/V_0$ against non-dimensional time $\tau := t/\tilde{t}$ (please note that τ is here redefined compared to section 2.1 with a minor abuse of notation), namely

$$\frac{\mathrm{d}\epsilon}{\mathrm{d}\tau} = A\,(1+\epsilon)^{-1} - \epsilon^3, \quad \epsilon\,(0) = 0. \qquad (8)$$

As for the piston implementation, the solution of problem (8) monotonically increases from the initial value up to a regime value ϵ_∞, which satisfies the equilibrium condition $A = \epsilon_\infty^3\,(1+\epsilon_\infty)$. Moreover, by observing that ϵ almost linearly increases versus τ (with slope A) for small values of τ, it is possible to estimate a characteristic timescale τ_c for the exponential decay of $\epsilon_\infty - \epsilon$, as follows: $A\tau_c \approx \epsilon_\infty$, whence (for ϵ_∞ small enough) $\tau_c \approx A^{1/3}/A = A^{-2/3}$. The differential problem (8) can be numerically integrated through standard methods (see, e.g., Press *et al* 1992). However, consistent with the small bulging deformation hypothesis (and by assuming 'reasonable' implementations), we are interested in solutions ϵ small enough (compared to 1), say $\epsilon_\infty \lesssim 10^{-1}$. This implies that $A \lesssim 10^{-3}$, as obtained from the above equilibrium condition. In the light of this observation, it is possible to approximate $\epsilon(\tau; A)$ with an analytical expression $\theta(\tau; A)$, i.e. $\epsilon \cong \theta$, which solves a simplified differential problem derived from (8) by truncation. Details regarding the considered derivation are reported in the appendix, for ease of presentation, while the resulting expression for θ is recalled hereafter:

$$\left(3\theta_\infty^2 + A\right)\tau = \log_{\mathrm{e}}\left[\frac{\Phi(0; A)}{\Phi(\theta; A)}\right] + \Omega(\theta; A) - \Omega(0; A)\,, \qquad (9a)$$

with

$$\theta_\infty(A) := \left(\frac{A}{2}\right)^{1/3}\left\{\left[1 + \sqrt{1 + \frac{4}{27}A}\right]^{1/3} + \left[1 - \sqrt{1 + \frac{4}{27}A}\right]^{1/3}\right\}, \qquad (9b)$$

$$\Phi(\xi; A) := \frac{\theta_\infty - \xi}{\sqrt{\xi^2 + \theta_\infty\xi + \theta_\infty^2 + A}}, \qquad (9c)$$

$$\Omega(\xi; A) := \frac{3\theta_\infty}{\sqrt{3\theta_\infty^2 + 4A}}\tan^{-1}\left(\frac{2\xi + \theta_\infty}{\sqrt{3\theta_\infty^2 + 4A}}\right). \qquad (9d)$$

The solution (9) accurately approximates ϵ over the considered range of the parameter A, as shown in the appendix. Exemplificative trends for the provided solution are shown in figure 5, for some values of the parameter A. For each curve, the filled circle is associated with the abscissa $t_{c,\mathrm{BM}}/\tilde{t}$, where $t_{c,\mathrm{BM}}$ is a characteristic time associated with the considered actuation dynamics. More precisely, it is derived from the left-hand-side term of equation (9a), by imposing $\left(3\theta_\infty^2 + A\right)\tau \cong t/t_{c,\mathrm{BM}}$, whence $t_{c,\mathrm{BM}} \cong \tilde{t}/\left(3\theta_\infty^2 + A\right)$.

Clearly, the main asset enabled by the obtained closed-form representation (9) is the possibility of studying how the considered dynamics depends on the involved parameters, through directly computable expressions. Relevant figures of merit for the actuation problem at hand are characteristic time ($t_{c,\mathrm{BM}}$), maximum force ($F_{\max}$), peak power ($P_{\max}$), power density ($\mu_P := P_{\max}/V_0$), cumulated work (W) and energy density ($\mu_W := W/V_0$). Corresponding scaling laws are reported in the appendix (see, in particular, table A.1), for ease of presentation.

3. Results and discussion

In this section, we elaborate on the membrane bulging model introduced in section 2.2, in view of its potential for prototypical development and experimental testing. In particular, we draw some preliminary design considerations, by exploiting the scaling laws reported in the appendix.

By recalling the typical pressure associated with plant roots penetration in soil (Zhu and Boyer 1992), we preliminarily adopt $\Pi_0 = 10^6$ Pa. Conversely, as regards the OM, it may not be suitable to derive a reference value for α_{OM} from data regarding cell walls in plant roots, since natural membranes also involve active transport mechanisms (for e.g. ion gate protein and special osmotic metabolism (Maurel 1997)). This, in turn, generally lowers the membrane rejection capabilities against solute transport, thus leading to membrane behaviour quite far from ideal. Therefore, in view of subsequent experimental testing, it seems suitable to consider commercially available membranes designed to operate with forward and pressure-retarded osmotic processes (Cath *et al* 2006), i.e. optimized for solvent fluxes $\dot{q}$ entering the AC like the one sketched in figure 1. Relevant items on the market, almost uniquely produced by HTI™ (Hydration Technology Innovations, Scottsdale, AZ, USA), are made up of cellulose polyacetate and exhibit a water permeability coefficient of around 3×10^{-13} m s^{-1} Pa^{-1}. Moreover, they are suitable for operation with sodium chloride (NaCl), since the corresponding rejection coefficient (which is 1 in the perfectly semi-permeable case) is in the range 0.95–0.97 (from datasheet) and they exhibit marginal performance degradation due to fouling. Both these aspects support the working hypotheses (h1) and (h2) introduced in section 2. Hence, for the present purposes it is reasonable to adopt $\alpha_{OM} = 3 \times 10^{-13}$ m s^{-1} Pa^{-1}, with reference to an existing commercial OM. It should be remarked that the above reference to NaCl is purposely introduced in view of subsequent experimental testing. Indeed, almost ideal osmotic behaviour can be achieved by using NaCl within water, thanks to the fact that NaCl is perfectly dissociated in water and it exhibits no significant deviations from the van't Hoff law (i.e. equation (1), with $i = 2$) (Marshall *et al* 1996). Moreover, the use of NaCl as a solute permits containment of the fouling effect on the OM (Mi and Elimelech 2008), which has consequent detrimental effects on the performance of the envisaged osmotic actuator. Fouling effects, in fact, may play a more major role for artificial membranes than in plant roots, where they are partly hindered by the dynamic nature of cell wall harnessing enzymes for the production of new cellulose (Cosgrove 2005). Finally, still in view of subsequent experiments, it is convenient to also estimate k_{BM}. To the purpose, we can invoke bioinspiration by looking to the cell wall of common plant roots, whose Young modulus is typically around 10^9 Pa (Gibson and Ashby 1999, Gibson *et al* 2010). Hence, by considering Cellophane™ as a reference material for the bulging membrane (having Young modulus $E \cong 3 \times 10^9$ Pa (Mark 2009) and the Poisson coefficient $\nu \cong 0.3$ (Nakamura *et al* 2004)) and by assuming a membrane thickness $t_{BM} \cong 3 \times 10^{-5}$ m (as for many commercially available films), we end up with the estimate $k_{BM} \cong 2.7 \times 10^7$ Pa m.

Let us then address the actuator size, by defining $L := S_{OM}^{1/2}$, $\lambda := V_0/S_{OM}^{3/2}$ and $\beta := S_{BM}/S_{OM}$. It should be noted that L provides a characteristic size for the actuator portion where solute transport takes place (being thus related to surface effects), while λ accounts for the relative importance between volume and surface effects. Moreover, for reasonable implementations, $0 < \beta < 1$. That said, it is immediate to obtain $A = \left(\Pi_0\beta^5 L\right) / \left(k_{BM}\lambda^3\right)$ and $\tilde{t} = \left(\beta^5 L^2\right) / \left(\alpha_{OM} k_{BM}\lambda^2\right)$, and to recast the actuator figures of merit (we make use of the simplified scaling laws in table A.1, for ease of presentation) as follows:

$$t_{c,BM} \cong \frac{1}{3\alpha_{OM} k_{BM}^{1/3}\Pi_0^{2/3}}\beta^{5/3}L^{4/3}, \tag{10}$$

$$F_{max} \cong \Pi_0 \beta L^2, \tag{11}$$

$$P_{max} \cong \frac{\Pi_0^2\alpha_{OM}}{4}L^2 \Rightarrow \mu_P \cong \frac{\Pi_0^2\alpha_{OM}}{4}\frac{1}{\lambda L}, \tag{12}$$

$$W \cong \frac{\Pi_0^{4/3}}{4k_{BM}^{1/3}}\beta^{5/3}L^{10/3} \Rightarrow \mu_W \cong \frac{\Pi_0^{4/3}}{4k_{BM}^{1/3}}\frac{\beta^{5/3}L^{1/3}}{\lambda}. \tag{13}$$

Furthermore, it is possible to estimate the bulging parameter $\delta/r \cong 2\sqrt{\pi}V_{BM}/S_{BM}^{3/2}$ as follows:

$$\frac{\delta}{r} \cong \frac{2\sqrt{\pi}\,\Pi_0^{1/3}}{k_{BM}^{1/3}}\beta^{1/6}L^{1/3}. \tag{14}$$

Based on the above relations, at the first approximation λ only affects power density μ_P and energy density μ_W in a simple way. Equations (12) and (13) show that optimal power and energy densities are achieved by minimizing λ (the minimum value which can be effectively attained in a practical implementation clearly depends on technological constraints, whose discussion is beyond the present scope). Furthermore, equation (12) shows that power consumption can be reduced by reducing L. Conversely, equations (10) and (11) show that greater/lower values of β and L lead to greater/lower values for both actuation characteristic time and maximum force. Hence, a trade-off between lower-yet-stronger and faster-yet-weaker actuation must be accepted, based on further design targets/constraints. If, for instance, we primarily target a specific actuation time, we can firstly use equation (10) in order to link β and L; then, we can compute the corresponding maximum force by exploiting equation (11), as exemplified in figure 6. In this figure, dotted curve portions denote less reliable model predictions, being associated with $\delta/r \gtrsim 0.2$ based on equation (14). For instance, a 1 min characteristic time can be achieved by choosing $L \cong 5$ mm (hence $S_{OM} \cong 25$ mm^2) and $S_{BM}/S_{OM} \cong 0.4$ or $L \cong 10$ mm (hence $S_{OM} \cong 100$ mm^2) and $S_{BM}/S_{OM} \cong 0.2$ (corresponding values for F_{max} are around 10 and 20 N, respectively).

If, instead, we primarily target a specific maximum actuation force, we can firstly use equation (11) in order to link β and L; then, we can compute the corresponding characteristic time through equation (10), as exemplified in figure 7 (as in the previous figure, the dotted curves denote less reliable model

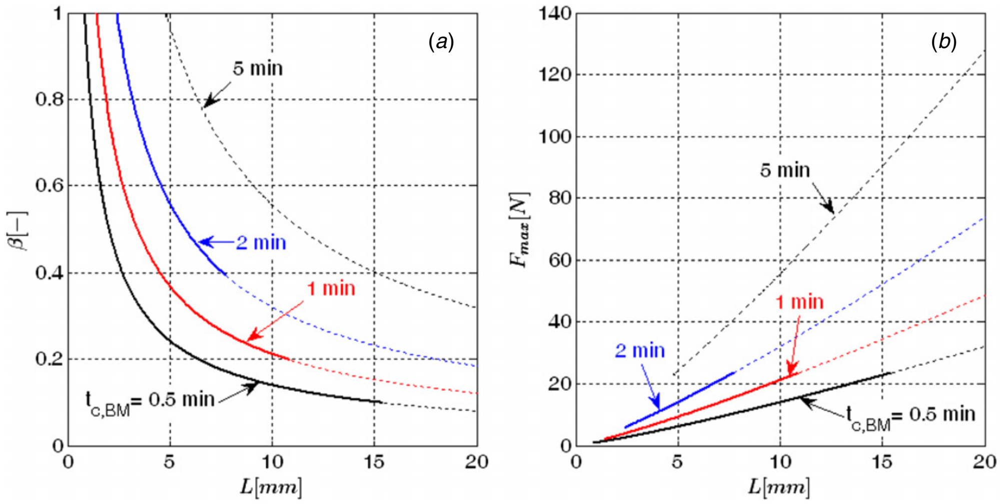

Figure 6. (*a*) Curves at constant characteristic time ($t_{c,\mathrm{BM}}$) a one-to-one relation between β and L is obtained from equation (10). (*b*) Corresponding maximum force ($F_{\max}$), as obtained from equation (11) by also considering the β–L. relation. Fixed model parameters: $\Pi_0 = 10^6$ Pa, $\alpha_{\mathrm{OM}} = 3 \times 10^{-13}$ m s^{-1} Pa^{-1}, $k_{\mathrm{BM}} = 2.7 \times 10^7$ Pa m.

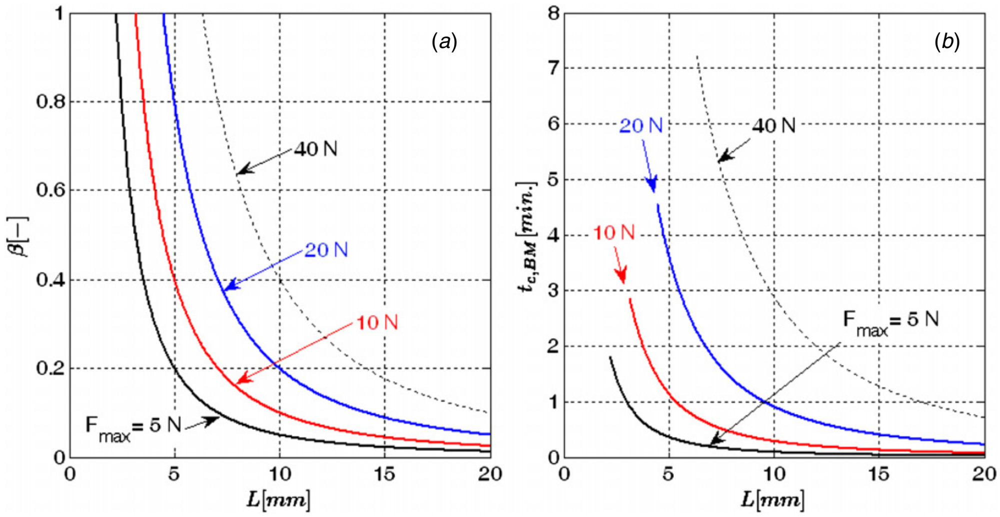

Figure 7. (*a*) Curves at constant maximum force ($F_{\max}$): a one-to-one relation between β and L is obtained from equation (11). (*b*) Corresponding characteristic time ($t_{c,\mathrm{BM}}$), as obtained from equation (10) by also considering the β–L relation. Fixed model parameters: $\Pi_0 = 10^6$ Pa, $\alpha_{\mathrm{OM}} = 3 \times 10^{-13}$ m s^{-1} Pa^{-1}, $k_{\mathrm{BM}} = 2.7 \times 10^7$ Pa m.

predictions, being associated with $\delta/r \gtrsim 0.2$). For instance, a 20 N maximum force can be achieved by choosing $L \cong 5$ mm (hence $S_{\mathrm{OM}} \cong 25$ mm^2) and $S_{\mathrm{BM}}/S_{\mathrm{OM}} \cong 0.8$ or $L \cong 10$ mm (hence $S_{\mathrm{OM}} \cong 100$ mm^2) and $S_{\mathrm{BM}}/S_{\mathrm{OM}} \cong 0.2$ (corresponding values for $t_{c,\mathrm{BM}}$ are around 3.5 and 1 min, respectively).

Expressions (10)–(13) permit us to also assess the influence of the remaining model parameters (i.e. those fixed above). For instance, increasing Π_0 would be beneficial for reducing characteristic time and for increasing maximum force, as well as power, power density, cumulated work and energy density. However, the solubility limit of the adopted solute possesses an upper bound on Π_0, and (having in mind, e.g., NaCl for effectively carrying out experimental tests) the adopted value seems to be a reasonable reference. Moreover, as anticipated at the beginning of this section, OM permeability is practically fixed. However, greater α_{OM} values would lead to reduced characteristic time and increased power and power density. Conversely, the stiffness of the bulging membrane might be negotiated. For instance, it can be verified from equations (10) and (11) that increasing k_{BM} by a factor 10 would increase the maximum force (at given $t_{c,\mathrm{BM}}$) in figure 6(*b*) by a factor $10^{1/5} \cong 1.6$, and reduce the characteristic times (at given $F_{\max}$) in figure 7(*b*) by a factor $10^{1/3} \cong 2.2$. Corresponding reduction in μ_W is mainly due to the reduced bulge volume.

Main limitations of the proposed model concern the ideal description of the osmotic process and the working hypothesis of small bulging deformations originally exploited for model derivation. As regards osmosis, it was anticipated at the beginning of the present section that rather ideal osmotic behaviour can be achieved by considering common solutions, such as sodium chloride in water, together with commercially available membranes designed for forward osmosis. Indeed, for sodium chloride in water the van't Hoff law nicely applies;

conversely, other inorganic salts with even greater van't Hoff coefficients exhibit lower water solubility and/or lower water solution stability, while also producing undesired stony by-products. Moreover, sodium chloride also leads to contained fouling effects with available osmotic membranes like the ones mentioned at the beginning of the present section. Other solutes such as sucrose (which can be effectively rejected by the aforementioned membranes as well) may cause detrimental effects on performance. For this reason, despite being the main solute for osmosis in plant root's tissue, sucrose does not seem to be a promising candidate for subsequent experimental testing (this is nonetheless consistent with the fact that the cellular wall does not represent an ideal source of inspiration for the present study, as remarked above). Furthermore, it is not realistic to fully neglect solute rejection by the OM: relevant diffusion dynamics might be considered in more elaborate models, depending on characteristic times. In addition, it was assumed that the whole bulk solute concentration drives the osmotic flux (see hypothesis (h3) at the beginning of section 2), thus likely underestimating surface effects close to the OM. This assumption, indeed, led to the lumped parameter approximation at the base of equation (3) (as well as to some derived results like the fact that, at a first approximation, actuation characteristic time only weakly depends on λ), yet it suitably applies to actuator configurations with a small aspect ratio λ only. However, it seems advisable to refine these modelling aspects in a further version of the model, e.g. by also considering membrane polarization effects (Cath *et al* 2006), which usually hamper the OM performances. Moreover, as regards small bulging deformations, it is worth remarking that they were assumed in order to introduce very simple analytical relations leading to model closure, otherwise very hard to achieve. Indeed, finite deformations of a bulging membrane should be tackled with more refined numerical modelling techniques, not commensurate with the simple approach deliberately pursued in this study. Nonetheless, these aspects should be included in a further version of the model, in order to take full advantage of the bulging implementation. This way one could also release the underlying assumption of uniform bi-axial tension, which is systematically violated towards the membrane boundary (so that the corresponding approximation gets less accurate for small S_{BM}). Finally, it should be noted that the assumption of negligible OM deformation during the actuation process (hypothesis (h4) at the beginning of section 2) was exploited from the first model derivation steps (for both piston and bulging implementations). However, it is worth emphasizing that even if OM deformations could be modelled through additional relations (e.g. derived from plate/membrane theory), they are deliberately unwanted in the considered osmotic process, since they would lead to incorrect dynamics (the displaceable/deformable surface S_w introduced in section 2 is indeed conceptually different from any OM portions). In fact, when such a hypothesis is not fulfilled, it is possible to observe an AC volume increment even without the presence of any deformable boundary portion S_w, as e.g. in Chahine *et al* (2005). Hence, suitable fastening of the OM plays a crucial role for practical implementations.

To summarize (and with focus on the bulge implementation), the proposed model permits us to draw some preliminary design considerations, starting from the scaling laws which were obtained for the actuation figures of merit. For instance, once relevant parameters (namely the initial osmotic pressure difference Π_0, the OM permeability coefficient α_{OM} and the bulging membrane stiffness k_{BM}) are fixed, it us permits to define a characteristic size $L = S_{\mathrm{OM}}^{1/2}$ (and the corresponding surface ratio $\beta = S_{\mathrm{BM}}/S_{\mathrm{OM}}$) for obtaining a given actuation characteristic time and a corresponding maximum force (or vice versa). For instance, if we pursue a 1 min characteristic time (with the parameters fixed in figure 6) and we aim at obtaining a maximum force around 10 N, we should choose $L = 5$ mm (related β is around 0.4). Furthermore, by minimizing the aspect ratio $\lambda = V_0/S_{\mathrm{OM}}^{3/2}$ (always in consideration of proper technological constraints), a power-dense and energy-dense actuator is achieved. In other words, the proposed model provides simple analytical expressions for obtaining a preliminary dimensioning of the envisaged osmotic actuator, based on design targets/constraints. This seems to support the choices which were made for model derivation, including the scaling quantities and non-dimensional model parameters. Within the limits of the adopted approximations, the main take home messages are to use targeted performances (primarily characteristic time and maximum force) for defining surface-related design parameters (like L and β) and to minimize the volume-to-surface aspect ratio λ, as permitted by additional (primarily technological) constraints. Experimental testing is nonetheless necessary for validating model predictions; having already in mind some key ingredients (e.g. to use sodium chloride in water, to adopt the aforementioned commercial OM ...), actuator prototyping and actuator performance assessment will be carried out in the near future.

4. Concluding remarks

Actuation currently represents a bottleneck for the development of many engineering systems. In particular, there is a growing quest for low power consumption and energy efficient actuation strategies, for which a remarkable source of inspiration is provided by the plant kingdom. Indeed, plant (non-muscular) movements are typically characterized by remarkable energy efficiency, high actuation force and a rich motion repertoire; all these aspects synergistically support plant survival in challenging dynamic environments. In the light of these considerations, suitable comprehension of plant osmotic-driven actuation strategies holds potential for the development of innovative biomimetic actuators, with application to many fields, including biorobotics.

This study takes a preliminary step towards the development of innovative osmotic-driven actuators, by analysing a concept simple enough to allow for modelling elaborations, while retaining the main physical phenomena involved in the osmotic process. In particular, some degree of simplification was introduced in order to keep analytical tractability; moreover, two implementations were presented, differing from each other in the way of achieving storage of the osmotic actuation work. We presented analytical solutions for both implementations, yet we only elaborated on the latter, in the light of its potential for effective prototypical development and experimental testing. In more detail, our approach permitted us to obtain explicit scaling laws for the actuation figures of merit, namely characteristic time, maximum force, peak power, power density, cumulative work and energy density. We showed how to use these expressions in order to draw some basic design considerations, by exemplifying a preliminary dimensioning of the envisaged osmotic actuator based on design targets/constraints (e.g. assigned actuation characteristic time and/or maximum force). The role of the volume-to-surface aspect ratio was also elucidated, with reference to actuator performance. Upon actuator prototyping, it is expected to experimentally assess model predictions in the short period; for this purpose, several elements necessary for experimental testing were already identified. In this spirit, the proposed modelling approach provides 'icebreaking' tools which can be effectively used for preliminary design, in particular, for the cheap exploration of a wide set of actuator configurations, to be incrementally refined during design and subsequent optimization. In addition, the identification of suitable interfaces for transferring the actuation work to the target environment will permit us to better specify the displaceable/deformable portion of the AC and the associated load conditions, thus further defining an actuator configuration to be optimized during later design stages. Nonetheless, mastery over the osmotic process harnessed in a proper actuator design holds potential for the development of controllable actuation strategies outperforming the passive ones proposed so far. Hence, the proposed study represents the first step on a challenging yet promising research path towards the development of innovative biorobotic solutions inspired by the plant kingdom.

Acknowledgments

The PLANTOID project acknowledges the financial support of the Future and Emerging Technologies (FET) programme within the Seventh Framework Programme for Research of the European Commission, under FET-Open grant number: 293431.

Appendix

For design purposes, it is convenient to replace (8) with a problem which can be analytically solved, since the latter generally leads to explicit relations for the actuator dynamics/performance as a function of the involved parameters. To this aim, we can truncate the expansion $(1+\epsilon)^{-1} \cong 1-\epsilon+\epsilon^2-\epsilon^3+\cdots$ so as to define an approximate problem, and adopt the solution to such a problem in order to approximate the 'exact' solution ϵ. For instance, a first-order truncation leads to the following problem (we denote the dependent variable by θ to stress the fact that we are addressing a 'new' problem):

$$\frac{\mathrm{d}\theta}{\mathrm{d}\tau} = A\,(1-\theta) - \theta^3, \quad \theta\,(0) = 0. \tag{A.1}$$

The regime value θ_∞ is given by the real root of the equilibrium equation $A\,(1-\theta) - \theta^3 = 0$ (it can be shown that there is a unique real root): the sought expression is reported in (9*b*). In particular, $A\,(1-\theta) - \theta^3 = (\theta_\infty - \theta)\left(\theta^2 + \theta_\infty\theta + \theta_\infty^2 + A\right)$, so that (A.1) can be integrated by the separation of variables as follows:

$$\mathrm{d}\tau = \frac{\mathrm{d}\theta}{A\,(1-\theta)-\theta^3} \Rightarrow \int_0^\tau \mathrm{d}\eta = \int_{\theta(0)=0}^{\theta} \frac{\mathrm{d}\omega}{(\theta_\infty-\omega)\left(\omega^2+\theta_\infty\omega+\theta_\infty^2+A\right)}, \tag{A.2}$$

where the integrals (involving rational functions) can be explicitly computed by recalling classical results, see e.g. Jeffrey and Zwillinger (2007). The obtained solution is reported in (9). Alternatively, one could have considered a zero-order truncation leading to the equation $\mathrm{d}\theta/\mathrm{d}\tau = A - \theta^3$ in place of the one in (A.1); the corresponding solution can be obtained as for the first-order truncation case (it is omitted, for brevity). Clearly, solution (9) is expected to better approximate ϵ compared to that based on zero-order truncation. However, whether its accuracy is enough for the present purposes (or, conversely, if it is necessary to perform higher order truncation) must be assessed; this is done below, also based on relevant figures of merit of the considered dynamic actuation model.

As anticipated in section 2.2, characteristic actuation time $t_{c,\mathrm{BM}}$ is derived from the left-hand-side term of equation (9*a*) by imposing $\left(3\theta_\infty^2 + A\right)\tau \cong t/t_{c,\mathrm{BM}}$, whence $t_{c,\mathrm{BM}} \cong \tilde{t}/\left(3\theta_\infty^2 + A\right)$. Moreover, actuation force is provided by $F = (p - p_{ext})\,S_{\mathrm{BM}} = \left(k_{\mathrm{BM}}V_0^3/S_{\mathrm{BM}}^4\right)\epsilon^3 = (\Pi_0 S_{\mathrm{BM}}/A)\,\epsilon^3 \cong (\Pi_0 S_{\mathrm{BM}}/A)\,\theta^3$, whence maximum force reads $F_{\max} \cong \Pi_0 S_{\mathrm{BM}}\left(\theta_\infty^3/A\right)$. Furthermore, power is given by $P = (p - p_{\mathrm{ext}})\,(\mathrm{d}V_{\mathrm{BM}}/\mathrm{d}t) = \left(\Pi_0 V_0/\left(A\tilde{t}\right)\right)\epsilon^3\,(\mathrm{d}\epsilon/\mathrm{d}\tau) \cong \left(\Pi_0 V_0/\left(A\tilde{t}\right)\right)\theta^3\,(\mathrm{d}\theta/\mathrm{d}\tau) = \left(\Pi_0 V_0/\left(A\tilde{t}\right)\right)\theta^3\left(A\,(1-\theta)-\theta^3\right)$. Peak power $P_{\max}$ is then obtained by maximizing the latter expression with respect to θ (since θ monotonically increases in time, so that there is a one-to-one relation between them). An analytical expression can also be obtained in this case; it is not reported here for simplicity, yet it is suitably approximated in table A.1. Power density is then defined as $\mu_P := P_{\max}/V_0$. Moreover, elementary actuation work is given by $\mathrm{d}W = (p - p_{\mathrm{ext}})\,\mathrm{d}V_{\mathrm{BM}} = \left(k_{\mathrm{BM}}V_0^3/S_{\mathrm{BM}}^5\right)\epsilon^3 V_0\,\mathrm{d}\epsilon = (\Pi_0 V_0/A)\,\epsilon^3\,\mathrm{d}\epsilon$, whence actuation work (up to regime) reads $W = (\Pi_0 V_0/4)\left(\epsilon_\infty^4/A\right) \cong (\Pi_0 V_0/4)\left(\theta_\infty^4/A\right)$. Finally, energy density is defined as $\mu_W := W/V_0$. By exploiting the solution (9), we report the aforementioned expressions in the left column of table A.1. However, by making use of the approximation in (A.3), we report approximate relations (terms A^n with $n \geqslant 1$ are neglected in the relevant expansions), for the sake of simplicity. Corresponding expressions, as derived from the above cited solution based on zero-order truncation, are also reported in the right column of table A.1, for the sake of comparison (see below).

Finally, figure A.1 shows the relative error on bulging volume at regime, power density and energy density, which is introduced by approximating ϵ with θ. In order to obtain such an error, the 'exact' solution ϵ was firstly determined by numerically integrating (8) through an adaptive, fourth-order accurate Runge–Kutta scheme (Press *et al* 1992), by choosing a strict relative tolerance (namely 10^{-12}). Derived figures of merit were then compared with the expressions

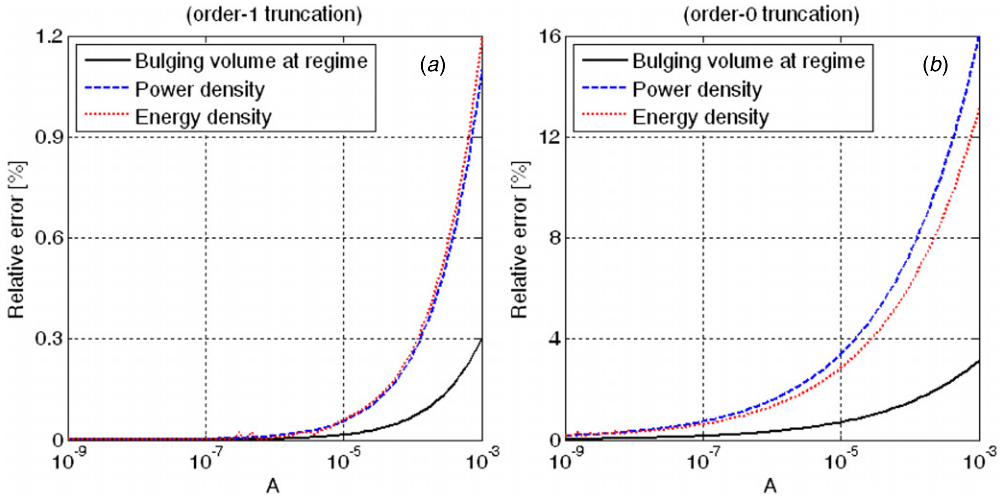

Figure A1. Relative error in bulging volume at regime, power density and energy density, introduced by the approximate solution θ versus the 'exact' one ϵ. (*a*) Error associated with first-order truncation. (*b*) Error associated with zero-order truncation.

Table A.1. Actuation figures of merit, as derived from the analytical expression of the approximate solution θ.

Solution (9) based on first-order truncation		Solution based on zero-order truncation	
$\theta_\infty = [\text{cf } (9b)] \cong A^{1/3}\left(1 - \frac{1}{3}A^{1/3}\right)$	(A.3)	$\theta_\infty = A^{1/3}$	(A.10)
$t_{c,\text{BM}} \cong \frac{1}{3}\tilde{t}A^{-2/3}\left(1 + \frac{1}{3}A^{1/3}\right)$	(A.4)	$t_{c,\text{BM}} \cong \frac{1}{3}\tilde{t}A^{-2/3}$	(A.11)
$F_{\max} \cong \Pi_0 S_{\text{BM}}\left(1 - 3A^{1/3} + 3A^{2/3}\right)$	(A.5)	$F_{\max} \cong \Pi_0 S_{\text{BM}}$	(A.12)
$P_{\max} \cong \frac{\Pi_0 \text{V}_0}{4}\tilde{t}^{-1}A\left(1 - 2\left(\frac{A}{2}\right)^{1/3} + \frac{16}{9}\left(\frac{A}{2}\right)^{2/3}\right)$	(A.6)	$P_{\max} \cong \frac{\Pi_0 \text{V}_0}{4}\tilde{t}^{-1}A$	(A.13)
$\mu_P \cong \frac{\Pi_0}{4}\tilde{t}^{-1}A\left(1 - 2\left(\frac{A}{2}\right)^{1/3} + \frac{16}{9}\left(\frac{A}{2}\right)^{2/3}\right)$	(A.7)	$\mu_P \cong \frac{\Pi_0}{4}\tilde{t}^{-1}A$	(A.14)
$W \cong \frac{\Pi_0 \text{V}_0}{4}A^{1/3}\left(1 - \frac{4}{3}A^{1/3} + \frac{2}{3}A^{2/3}\right)$	(A.8)	$W \cong \frac{\Pi_0 \text{V}_0}{4}A^{1/3}$	(A.15)
$\mu_W \cong \frac{\Pi_0}{4}A^{1/3}\left(1 - \frac{4}{3}A^{1/3} + \frac{2}{3}A^{2/3}\right)$	(A.9)	$\mu_W \cong \frac{\Pi_0}{4}A^{1/3}$	(A.16)

in table A.1, namely (A.3), (A.7) and (A.9), and (A.10), (A.14) and (A.16), for the respective θ solutions. It turned out that solution (9), based on first-order truncation, provides an accurate approximation over the considered range of A (so that it is not necessary to consider higher order truncation, leading in turn to more involved and less expressive formulas). Estimates obtained from zero-order truncation are nonetheless useful for preliminary design, as exemplified in section 3.

References

Andersson H and van den Berg A 2003 Microfluidic devices for cellomics: a review *Sensors Actuators* B **92** 315–25

Atkins P W 1994 *Physical Chemistry* 5th edn (Oxford: Oxford University Press)

Baskin T I 2005 Anisotropic expansion of the plant cell wall *Annu. Rev. Cell Dev. Biol.* **21** 203–22

Bengough A G, Croser C and Pritchard J 1997 A biophysical analysis of root growth under mechanical stress *Plant Soil* **189** 155–64

Burgert I and Fratzl P 2009 Actuation systems in plants as prototypes for bioinspired devices *Phil. Trans. R. Soc. Lond.* A **367** 1541–57

Cath T Y, Childress A E and Elimelech M 2006 Forward osmosis: principles, applications, and recent developments *J. Membr. Sci.* **281** 70–87

Chahine N O, Chen F H, Hung C T and Ateshian G A 2005 Direct measurement of osmotic pressure of glycosaminoglycan solutions by membrane osmometry at room temperature *Biophys. J.* **89** 1543–50

Cosgrove D J 2005 Growth of plant cell wall *Nature Rev. Mol. Cell Biol.* **6** 850–61

Darwin C 1875 *Insectivorous Plants* (London: Murray)

Darwin C and Darwin F 1880 *The Power of Movements in Plants* (London: Murray)

Dumais J and Forterre Y 2012 'Vegetable dynamicks': the role of water in plant movements *Annu. Rev. Fluid. Mech.* **44** 453–78

Fahn A and Werker E 1972 Anatomical mechanisms of seed dispersal *Seed Biology* ed T T Kozlowski (New York: Academic) pp 151–221

Forterre Y, Skotheim J M, Dumais J and Mahadevan L 2005 How the Venus flytrap snaps *Nature* **433** 421–5

Fromm J and Lautner S 2007 Electrical signals and their physiological significance in plants *Plant Cell Environ.* **30** 249–57

Gibson L J and Ashby M F 1999 *Cellular Solids: Structure and Properties* (Cambridge: Cambridge University Press)

Gibson L J, Ashby M F and Harley B A 2010 *Cellular Materials in Nature and Medicine* (Cambridge: Cambridge University Press)

Gilroy S and Masson P H 2008 *Plant Tropisms* (Oxford: Blackwell)

Green P B, Erickson R O and Buggy J 1971 Metabolic and physical control of cell elongation rate: *in vivo* studies *Nitella Plant Physiol.* **47** 423–30

Hart J W 1990 *Plant Tropisms and Other Growth Movements* (London: Unwin Hyman)

Hill B S and Findlay G P 1981 The power of movement in plants: the role of osmotic machines *Q. Rev. Biophys.* **14** 173–222

Ince E L 1956 *Ordinary Differential Equations* reprint edn (New York: Dover)

Jeffrey A and Zwillinger D 2007 *Table of Integrals, Series, and Products* 7th edn (New York: Academic)

Jost L and Gibson R J H 1907 *Lectures on Plant Physiology* (Oxford: Clarendon)
Li Y-H and Su Y-C 2010 Miniature osmotic actuators for controlled maxillofacial distraction osteogenesis *J. Micromech. Microeng.* **20** 1–8
Mark J E 2009 *Polymer Data Handbook* 2nd edn (Oxford: Oxford University Press)
Marshall S L, May P M and Hefter G T 1996 Least-squares analysis of osmotic coefficient data at 25 °C according to Pitzer's equation. 1. 1:l electrolytes *J. Chem. Eng. Data* **40** 1041–52
Martone P T *et al* 2010 Mechanics without muscle: biomechanical inspiration from the plant world *Integr. Comp. Biol.* **50** 888–907
Maurel C 1997 Aquaporins and water permeability of plant membranes *Annu. Rev. Plant Physiol. Plant Mol. Biol.* **48** 399–429
Mazzolai B, Mondini A, Corradi P, Laschi C, Mattoli V, Sinibaldi E and Dario P 2011 A miniaturized mechatronic system inspired by plant roots for soil exploration *IEEE/ASME Trans. Mechatronics* **16** 201–12
Mi B and Elimelech M 2008 Chemical and physical aspects of organic fouling of forward osmosis membranes *J. Membr. Sci.* **320** 292–302
Moran N 2007 Osmoregulation of leaf motor cells *FEBS Lett.* **581** 2337–47
Moulia B and Fournier M 2009 The power and control of gravitropic movements in plants: a biomechanical and systems biology view *J. Exp. Bot.* **60** 461–86
Nakamura K, Wada M, Kuga S and Okano T 2004 Poisson's ratio of cellulose Iβ and cellulose II *J. Polym. Sci.* B **42** 1206–11
Oda K and Abe T 1972 Action potential and rapid movement in the main pulvinus of *Mimosa pudica J. Plant Res.* **85** 135–45
Piyasena M E, Newby R, Miller T J, Shapiro B and Smela E 2009 Electroosmotically driven microfluidic actuators *Sensors Actuators* B **141** 263–69
Popova L, Russino A, Ascrizzi A and Mazzolai B 2012 Analysis of movement in primary maize roots *Biologia* **67** 517–24
Press W H, Teukolsky S A, Vetterling W T and Flannery B P 1992 *Numerical Recipes in C: The Art of Scientific Computing* 2nd edn (Cambridge: Cambridge University Press)
Preston R 1974 *The Physical Biology of Plant Cell Walls* (London: Chapman and Hall)
Pritchard J 1994 The control of cell expansion in roots *New Phytol.* **127** 3–26
Roelfsema M R G and Hedrich R 2002 Studying guard cells in intact plant: modulation of stomatal movement by apoplastic factors *New Phytologist* **153** 425–31
Ruhland W 1959 *Encyclopaedia of Plant Physiology* vol 17*: Physiology of Movements* (Berlin: Springer)
Sibaoka T 1991 Rapid movements triggered by action-potentials *Bot. Mag. Tokyo* **104** 73–95
Simons P J 1981 The role of electricity in plant movements *New Phytol.* **87** 11–37
Skilhagen S E, Dugstad J E and Aaberg R J 2008 Osmotic power production based on the osmotic pressure difference between waters with varying salt gradients *Desalination* **220** 476–82
Small M and Nix W 1992 Analysis of the accuracy of the bulge test in determining the mechanical properties of thin films *J. Mater. Res.* **7** 326–35
Steudle E and Peterson C A 1998 How does water get through roots? *J. Exp. Bot.* **49** 775–88
Su Y-C *et al* 2002 A water powered osmotic microactuator *J. Microelectromech. Syst.* **11** 736–42
Taiz L and Zeiger E 2002 *Plant Physiology* 3rd edn (Sunderland, MA: Sinauer)
Taya M 2003 Bio-inspired design of intelligent materials *Proc. SPIE* **5051** 54–65
Theeuewes F and Yum S Y 1976 Principles of the design and operation of generic osmotic pumps for the delivery of semisolid or liquid drug formulations *Ann. Biomed. Eng.* **4** 343–53
Timoshenko S 1964 *The Theory of Plates and Shells* 2nd edn (New York: McGraw-Hill)
Uehlein N and Kaldenhoff R 2008 Aquaporins and plant leaf movements *Ann. Bot.* **101** 1–4
Wang C, Wang L, Zhu X, Wang Y and Xue J 2012 Low-voltage electroosmotic pumps fabricated from track-etched polymer membranes *Lab Chip* **12** 1710–6
Zhu G L and Boyer J S 1992 Enlargement in *Chara* studied with a turgor clamp: growth rate is not determined by turgor *Plant Physiol.* **100** 2071–80